HHS Public Access

Author manuscript

J Chem Inf Model. Author manuscript; available in PMC 2017 March 27.

Published in final edited form as:

J Chem Inf Model. 2016 December 27; 56(12): 2378–2387. doi:10.1021/acs.jcim.6b00095.

Genetic Algorithm Managed Peptide Mutant Screening: Optimizing Peptide Ligands for Targeted Receptor Binding

Matthew D. King[†], **Thomas Long**[‡], **Timothy Andersen**[‡], and **Owen M. McDougal**[*,†]

[†]Department of Chemistry Boise State University, 1910 University Drive, Boise, Idaho 83725, United States Biochemistry

[‡]Department of Computer Science, Boise State University, 1910 University Drive, Boise, Idaho 83725, United States

Abstract

This study demonstrates the utility of genetic algorithms to search exceptionally large and otherwise intractable mutant libraries for sequences with optimal binding affinities for target receptors. The Genetic Algorithm Managed Peptide Mutant Screening (GAMPMS) program was used to search an α-conotoxin (α-CTx) MII mutant library of approximately 41 billion possible peptide sequences for those exhibiting the greatest binding affinity for the $\alpha_3\beta_2$-nicotinic acetylcholine receptor (nAChR) isoform. A series of top resulting peptide ligands with high sequence homology was obtained, with each mutant having an estimated ΔG_{bind} approximately double that of the potent native α-CTx MII ligand. A consensus sequence from the top GAMPMS results was subjected to more rigorous binding free energy calculations by molecular dynamics and compared to α-CTx MII and other related variants for binding with $\alpha_3\beta_2$-nAChR. In this study, the efficiency of GAMPMS to substantially reduce the sample population size through evolutionary selection criteria to produce ligands with higher predicted binding affinity is demonstrated.

Graphical abstract

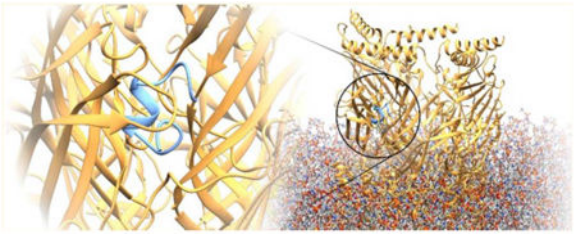

Introduction

Nicotinic acetylcholine receptors (nAChRs) are pentameric ligand-gated ion channels that play an important role in cognitive function and the prevention of neuronal degradation,

Corresponding Author: owenmcdougal@boisestate.edu.

Author Information: The authors declare no competing financial interest.

bringing investigations of these receptors to the forefront of research into neurodegenerative disorders such as Alzheimer's disease and Parkinson's disease.[1–4] Studies have demonstrated decreased levels of nicotinic receptors in post-mortem examinations of individuals previously afflicted with forms of dementia.[5] In contrast, epidemiological studies have demonstrated an inverse relationship between the development of neurodegenerative disorders and smoking as well as the influence of nicotine in the enhancement of cognitive function in animals, including humans.[6,7] Nicotine, an exogenous agonist and the namesake of nAChRs, triggers an active biological response upon binding that results in upregulation of neuronal receptors while reducing their susceptibility to proteasomal subunit degradation.[8,9] The well-established negative impacts of nicotine usage notwithstanding, there are great potential benefits in the development or discovery of alternative nAChR agonists for the treatment of patients with neuro-degenerative disorders.

Another class of ligand for nAChRs that has been extensively studied are α-conotoxins (α-CTx), which are neurotoxic peptides isolated from the venom of the marine snails of genus *Conus*.[10–12] α-CTx are small peptides consisting of 10– 30 amino acid residues that contain one or more disulfide bonds. Unlike nicotine, these small peptides have been found to selectively block specific nAChR subtypes.[13,14] For this reason, they have received a considerable amount of attention in the field of pharmacology as molecular probes for the structure– function relationships of nAChRs toward the goal of developing targeted therapeutics for neurodegenerative diseases.

Of particular interest, and the premise for this study, is α-CTx MII, a 16 amino acid peptide that exhibits an IC_{50} of 0.5 nM for the $\alpha_3\beta_2$-nAChR isoform.[13–15] αCTx MII has the primary sequence GCCSNPVCHLEHSNLC, contains two disulfide bonds (C2–C8 and C3–C16), and features an α-helix initiated at P6 and ending at S13 (Figure 1). This peptide has been the subject of many investigations aimed at developing a better understanding of the selectivity and potency of α-CTx MII and its variants. Some such studies have included site-directed mutagenesis of nAChRs, alterations of the primary sequence of α-CTx MII, and computational modeling using molecular docking and dynamics approaches.[12,16–20] Notably, several mutants of the α-CTx MII peptide have shown significant enhancement in binding affinity for the $\alpha_3\beta_2$-nAChR isoform as well as other nAChR isoforms, such as the E11A mutant, which demonstrated a 50-fold binding preference for the $\alpha_6\alpha_4\beta_2\beta_3$-nAChR isoform.[12,21]

α-CTx MII was selected as a template for a comprehensive search of custom peptide sequences with optimal binding affinity for the $\alpha_3\beta_2$-nAChR isoform because of its proven selectivity and potent inhibition of the receptor. The discovery of sequences with improved affinity to nAChR could increase the knowledge of the structure–function relationship consequential to neurodegenerative disorders. Understanding this relationship may also lead to the development of new non-peptide therapeutic agents based on structural similarities that are capable of the analogous binding affinity and specificity necessary for targeted drug treatments. The search for α-CTx MII mutants with high binding affinity for the $\alpha_3\beta_2$-nAChR was performed using the Genetic Algorithm Managed Peptide Mutant Screening (GAMPMS) method, a genetic algorithm designed for comprehensive structure-based high-throughput virtual screening (HTVS) of a very large mutant library.[22]

Genetic algorithms (GAs) have found application in computational and combinatorial chemistry.[23–26] While machine-learning-based scoring functions can be used in place of traditional docking methods in order to increase the throughput of a ligand database screen, they are often less accurate. Also, the reported score that is assigned by a learning algorithm to ligand–receptor binding may be of limited value in the context of the scientific community since the assigned scores are not directly reproducible because of custom implementations using unique training sets. In contrast, GAMPMS is an unsupervised GA that uses the results of previous docking jobs to make an informed decision as to which mutations increase or decrease peptide binding affinity. Additionally, the GAMPMS method uses the popular AutoDock 4.0 molecular docking software to provide fitness scores, giving it the added advantage of making the molecular docking results reproducible by other researchers.[27,28] A graphical representation of the GAMPMS workflow is shown in Figure 2, demonstrating how the three genetic operators derived from the natural evolutionary processes of elitism, crossover, and mutation are used in determining peptide sequences with the highest fitness (binding affinity).

GAMPMS was used to perform a combinatorial biochemistry experiment based on the α-CTx MII peptide utilizing structure-based HTVS methods in order to identify peptides with a higher predicted binding affinity for the $\alpha_3\beta_2$-nAChR. The implementation of GAMPMS permitted the search of a remarkably large mutation space of *40.96 billion* possible peptide sequences ($8^4 \times 10^7$ possible mutant combinations). The binding free energies of the resulting top-ranking sequences obtained from GAMPMS were compared to that of native MII, and a consensus amino acid sequence was generated on the basis of the residue conservation probabilities. Molecular dynamics simulations were used to support the GAMPMS results as well as to further investigate the binding interactions resulting in the predicted enhancement in binding affinity.

The implementation and capacity of GAMPMS in searching exceptionally large peptide mutant libraries is of great importance for the advancement of peptide therapeutic development and research in neurodegenerative disorders. The implications of fast and effective methods for database searching cannot be understated as drug discovery efforts increasingly move toward in silico modeling and sophisticated search algorithms to streamline the process of discovering novel therapeutic agents. Furthermore, the integration of GAMPMS and the associated programs into the DockoMatic software package makes this methodology readily available to the research community.[29]

Methods

Genetic Algorithm

The detailed implementation of GAMPMS integrated into the DockoMatic 2.1 software package is described elsewhere, so only a brief description is provided here.[22,29] The receptor structure used in docking calculations was a homology model of the $\alpha_3\beta_2$-nAChR isoform constructed from the amino acid sequences of the α_3 (UniProtKB ID P04757.1) and β_2 (P12390.2) subunits of rat neuronal nAChR using the *Torpedo marmorata* nAChR (PDB ID 2BG9) as a structural template.[30,31] The homology models were created using the DockoMatic 2.1[29] and MODELLER[32] packages. The amino acid sequences of $\alpha_3\beta_2$-nAChR

and the templates were aligned according to sequence similarity, and atomic coordinates were assigned to the models on the basis of sequence and structural alignment with the templates. This was followed by optimization of amino acid side-chain rotamers and steepest-descent energy optimization of the models. The constructed $\alpha_3\beta_2$ subunit dimer consisting of only the extracellular domains was used for subsequent computational studies, although nAChR exists naturally as a pentameric transmembrane protein complex.

Representation of an Individual—In the GA integrated into DockoMatic 2.1, each individual (peptide mutant) is represented as a sequence of amino acids that can be substituted for the base peptide's mutable residues (Table 1). The α-CTx MII sequence was used as the base sequence for mutation. The C2, C3, P6, C8, and C16 residues were conserved during their simulation because of their importance in conformational stability. The cysteine residues are involved in disulfide bonds, while the proline initiates α-helix formation. Allowed mutations were not expected to alter the secondary structure of the peptide template. Residue mutations were constrained to maintain the polar/nonpolar character of the residue. The polar and/or charged S4, N5, H9, E11, H12, S13, and N14 residues could mutate into polar and/or charged amino acids (excluding cysteine), and the nonpolar G1, V7, L10, and L15 residues could mutate into nonpolar amino acids (excluding proline).

Using the single-letter amino acid symbols, each individual is represented as a character array. Site-directed mutagenesis of individuals is handled by the Treepack program, which is included as part of DockoMatic 2.1. Three-dimensional peptide mutant structures are generated by the following process: (1) the coordinates of the mutable residue and two adjacent residues are copied into a new pdb file; (2) the side-chain atoms of the mutable residue are removed from the generated tripeptide pdb file; (3) the side-chain atoms of the substituted amino acid are added; (4) the peptide analogue is submitted to Treepack, which determines the appropriate orientation of the new side chain to eliminate side-chain spatial overlaps; (5) the modified peptide segment is grafted back into the original ligand pdb file. The fitness of an individual is determined by the AutoDock score produced when the ligand is docked against the target receptor.

Genetic Operators—Three basic genetic operators derived from the natural biological evolutionary process are implemented by GAMPMS: *elitism, crossover*, and *mutation*. The user-defined elitism operator is used to select the top *elite factor* × 100% of a population's individuals and add them to the successive population. The two-parent, two-offspring, N-point crossover operator uses a fitness-proportionate selection scheme, choosing two individuals (parents) from the current population with a probability directly proportional to their fitness ranking within the population. A set of N indices are chosen randomly from within a parent's range, and both parents are split into $N + 1$ pieces according to the indices. The pieces from the two parents are alternated and combined to make two different offspring that share features of both parents. For the genetic operator of mutation, an amino acid has an equal chance of changing into any of the other amino acids in the associated residue's substitution set at a rate specified by the user. The resulting populations after the three

genetic operations are performed on a parent population are used as subsequent input sequences for docking until the convergence criteria are achieved.

Terminating Condition—GAMPMS iteratively builds new populations until the specified convergence criteria are met. In DockoMatic 2.1, the genetic algorithm stops generating new populations when there has been no change in the top X highest-affinity peptides over the last λ iterations. The parameters X and λ are both configurable in DockoMatic 2.1.

GAMPMS of the 40 960 000 000 α-CTx MII Mutant Ligand Library

The GAMPMS model was implemented and used to search the 40 960 000 000 α-CTx MII mutant library for binding affinity to the $\alpha_3\beta_2$-nAChR. The search was performed using 128 cores on the Fission cluster at Idaho National Laboratory. Forty pose evaluations (ga_runs) were used in the AutoDock docking simulation for ligand–receptor binding. Had conventional HTVS been performed on the mutant library, an intractable 3.2×10^8 submissions would have been required (using 128 cores). Instead, the GAMPMS implementation required a total of only 19 041 molecular docking jobs to reach convergence. Input files for molecular docking were generated from pdb files using AutoDockTools, and docking was performed using AutoDock 4.0, both of which are integrated into DockoMatic. The GA was configured with an elitism carryover of the top 40% of each population, a two-parent, two-offspring, three-point crossover, and a mutation probability of 2%. The GA terminated after five iterations without an improvement in the binding energy of the top 50 peptides.

The top-ranking individuals of such a large mutation space produce estimated binding free energies that are within the accepted error of the AutoDock scoring functions.[28] Thus, the lowest-energy sequence cannot be taken as the “best” sequence. The well-documented uncertainty in values of predicted binding free energies from molecular docking scoring functions must be taken into consideration, and this is something that is often overlooked when molecular docking is applied in ligand– receptor binding studies. Since we are studying a highly variable peptide ligand, the best indicator that a side-chain mutation results in a beneficial effect on the predicted binding affinity is not the docking score directly but rather the conservation of any particular mutation that is observed among a population exhibiting the best docking scores. Therefore, the conservation of residues across the peptides with the highest binding affinities was used to determine the final top sequence. The residue occurring with the highest frequency in the top 50 peptides, with all residues having a conservation of at least 50%, was included in the consensus sequence (WCCSYPG-CYWSSSKWC). This peptide sequence was subjected to further investigation and validation using molecular dynamics (MD) simulations and compared to sequences with known binding affinities with the $\alpha_3\beta_2$-nAChR isoform.

Molecular Dynamics Simulations

MD simulations were performed using the Gromacs 5.0.4 software package with the AMBER03 force-field parameter set.[34–39] GAMPMS-derived molecular docking results were used as input structures for MD. Simulations were performed with periodic boundary conditions with explicit solvation using the transferable intermolecular potential 3-point

(TIP-3P) potential model.[40] To prepare the solvated systems for simulation, a conjugate-gradient energy minimization followed by *NVT* and *NPT* equilibrations was performed. A 100 ps equilibration was conducted under the *NVT* ensemble using a velocity-rescale thermostat at 300 K with a coupling time constant of 0.1 ps.[41,42] A subsequent 200 ps *NPT* equilibration was performed using the isotropic Parrinello–Rahman barostat with a time constant of 1.0 ps.[43] The integration time for both equilibration steps was 1 fs. An initial 50 ns MD simulation was executed for each system using an integration time step of 1 fs. All bonds were constrained to their equilibrium values using the LINCS algorithm.[44] Since only the extracellular $\alpha_3\beta_2$ dimer subset was used, position restraints with force constants of 5000 kJ mol^{-1} nm^{-2} were applied to the receptor residues on the interior portion of the dimer subunits, or what would be the ion channel side of the nAChR, opposite the α-CTx binding region. The Verlet cutoff scheme was used in the calculation of short-range Coulomb and van der Waals forces, and the particle-mesh Ewald method was employed for long-range electrostatics.[45,46] The structures averaged over the final 10 ns of each simulation run were used in the subsequent free energy simulations.

For MD calculations of binding free energy of each variant with $\alpha_3\beta_2$-nAChR, the classic thermodynamic cycle shown in Scheme 1 was used. The ΔG_{bind} term is the free energy of binding between the receptor and the ligand. ΔG_1 is the free energy change of the transition of the ligand from a bound state to a virtual (dummy) state in which all of the interaction terms have been turned off, and ΔG_2 is the free energy of the transition of the ligand from a solvated state to a dummy state. The relative binding free energy of the ligand with the nAChR, ΔG_{bind}, can be determined by calculating ΔG_1 and ΔG_2 and using the relationship $\Delta G_{bind} = \Delta G_1 - \Delta G_2$.

Simulation of state transitions from real to virtual states was implemented in two steps: (1) incrementally turning off the Coulombic interactions between the ligand and the receptor and (2) incrementally turning off the Lennard-Jones interactions between the ligand and the receptor. Calculations of intermediate λ states were performed at 11 and 21 equidistant nodes for steps 1 and 2, respectively. During decoupling of the van der Waals interactions, soft-core potential functions were applied with $\alpha_{LJ} = 0.5$ and the λ power dependence set to 1.[47] A harmonic restraint with a force constant of 100 kJ mol^{-1} nm^{-2} was placed between the receptor and ligand centers of mass to maintain the relative distance between the ligand and receptor in order to prevent unphysical repositioning of the ligand during the decoupling steps due to decreased interaction strengths. At each λ value, simulations were performed for 500 ps with a time step of 0.5 fs. $\partial H/\partial\lambda$ was saved every 10 fs for postprocessing and free energy calculations using the Bennett's acceptance ratio (BAR) perturbation method.[48,49] Only the last 250 ps of each simulation was used for BAR calculations, with the first 250 ps being considered as additional system equilibration. Four series of free energy simulations were performed for each ligand in the forward and backward (coupling and decoupling) directions for the receptor-bound ligand and solvated ligand.

Results and Discussion

The top 10 peptide sequences obtained from searching the 40.96 billion mutant library using GAMPMS are provided in Table 2. These results had estimated binding free energies

ranging from −22.26 to −23.45 kcal/mol. Comparison with the affinity of native α-CTx MII for the $\alpha_3\beta_2$-nAChR shows that the resulting binding free energies of the mutants are nearly double the ΔG_{bind} of-12.38 kcal/mol of MII, with $\Delta\Delta G$ ranging from −9.88 to −11.07 kcal/mol. The observed differences between the top mutants within the range of 1.19 kcal/mol are within the error range of free energies estimated by AutoDock 4.0 (~2.1 kcal/mol).[28] Thus, a definitive peptide sequence exhibiting the "best" binding affinity to the nAChR cannot be directly determined. However, examination of the top sequences produced by the genetic algorithm showed a high degree of sequence similarity, which is an important indicator of the mutations contributing most favorably to the overall ligand binding affinity.

On the basis of the estimated binding free energies producing by GAMPMS, the top 51 sequences fell within the standard error of the AutoDock scoring function. A series of top mutant population sizes were evaluated to determine the extent of residue conservation and to support the viability of generating a consensus sequence based on the observed probabilities of residue occurrences at all mutated positions. Populations of the top 10, 20, 30, 40, 50, and 60 mutants were examined, assuming statistical equivalence in the predicted binding affinities of all of the top peptide mutants. The same sequence resulted from each population when the highest frequency of any particular residue mutation was considered. Confidence intervals (CIs, α = 0.05) of residue mutation probabilities were generated for each population size. Only at N = 50 does the mutation of highest probability at each mutable residue lie outside the 95% CI of the second most frequently observed mutation, with the exception of residue 14 (although Lys14 occurs at the highest frequency in all populations). In addition, N = 50 is the largest population containing only resulting sequences within the standard error of the binding free energy estimates.

The bar graph in Figure 3 clearly shows the residue conservation for each mutable residue from the GAMPMS results. Each position, with the exception of residue 14, contained a single residue that appeared in a minimum of 50% of the top 50 sequences, with a tryptophan appearing at residue 10 in all of the sequences. The consensus sequence (KTM) produced from these findings was WCCSYPGCYWSSSKWC. Comparison of this sequence with the top 10 listed in Table 2 shows greater than 56% residue conservation in every case, 75% conservation with the top sequence, and a high of 81.25% conservation with the sixth-ranked sequence. The predicted binding free energy of the consensus sequence was −21.47 kcal/mol, which ranks the mutant in the top 50 sequences and within the standard error of the AutoDock scoring function of the top-ranked peptide.

The overall sequences and structures of native α-CTx MII and KTM are notably different (Figure 4). The only mutable residues conserved between MII and KTM are Ser4 and Ser13, giving a total of seven conserved residues when the nonmutated Cys and Pro residues are taken into account. The additions of bulky amino acid structures, particularly three Trp and two Tyr residues, have a significant impact on the size of the mutant peptide. A nearly 10% increase in molecular volume was calculated, from 1578 to 1732 $Å^3$ for α-CTx MII and KTM, respectively, with corresponding molecular weights of 1701 and 1835 Da. It is clear from Table 2 that each of the resulting top ligands has a higher molecular weight than the native α-CTx MII. While it is accepted that docking scores are biased toward molecules with higher molecular weights, the increases in predicted binding free energies of the top

ligands are significantly larger than can be explained by the less than 10% increase in molecular weight. Normalization of docking scores to correct for molecular weight using $\Delta G_{norm} = \Delta G_{bind}/N^{1/3}$, where N is the number of heavy atoms, yields normalized binding free energies of 2.55 and 4.58 kcal/mol for α-CTx MII and the top-ranking mutant from Table 2, respectively.[50] The molecular weight bias, although not a major factor in the docking results, is one of many concerns inherent in molecular docking approaches. Other limitations leading to ambiguity in energy rankings obtained from docking programs include binding pocket flexibility and dynamics, adequate sampling of the receptor and ligand conformational spaces, and desolvation energies. Molecular docking is powerful in that such methods may provide reasonable results and ligand docking orientations and, most importantly, can facilitate HTVS of large compound databases. However, to achieve more reliable binding free energies and further explore the interaction dynamics of receptor–ligand complexes, more robust computational methods are needed. The predicted binding affinities of the α-CTx MII and consensus KTM peptide ligands were further evaluated using molecular dynamics.

To initially evaluate the variations in binding interactions and pose between the two ligands, the two systems were subjected to 50 ns MD simulations. From these simulations, the accuracy of the docking pose provided by AutoDock and the primary interactions stabilizing the peptides within the nAChR binding pocket can be more closely examined. Molecular docking procedures offer only an estimate of the ligand binding free energy. Limitations are placed on molecular flexibility for both the ligand and receptor, which can lead to larger errors in predicted energies even with the implementation of rotatable bonds for residue side chains. In order to achieve reasonable values of binding free energies of ligand–receptor complexes, variability in all of the atomic positions directly and indirectly associated with the interactions is a necessity to allow the structures to relax and reach an energetic minimum. The dynamics of large biomolecular structures cannot be disregarded when attempting to quantify binding energies. That said, molecular docking does provide a reasonable estimation of energy rankings or docking scores, and these methods can be used to determine significant differences in favorable binding interactions. However, to obtain more accurate measures of actual molecular processes, more robust methods, such as molecular dynamics, are necessary.

With the docking poses obtained from the molecular docking calculations, 50 ns MD simulations were performed for both the α-CTx MII and KTM ligands bound to the nAChR. Both ligands showed a high degree of stability in their binding configurations, as evidenced by the root-mean-square deviations (RMSDs) of ligand atomic positions over 50 ns (Figure 5). Some fluctuations were observed over the 50 ns simulations as the ligands sampled conformational space within the binding pocket to achieve more favorable interactions with the nAChR. As shown in Figure 6, the number of stabilizing hydrogen bonds increased for both ligands over 50 ns. The number of hydrogen bonds formed between KTM and the nAChR within a 3.5 Å cutoff distance was notably larger than that for α-CTx MII, with the number fluctuating around nine for KTM and six for α-CTx MII. This increased electrostatic interaction of KTM with the nAChR should correlate to a significantly greater binding affinity.

The primary hydrogen-bonding interactions for the two ligands bound to the nAChR are shown in Figure 7. The hydrogen bonding of MII is exclusively to the β_2 subunit, whereas the hydrogen bonding of KTM involves both the α_3 and β_2 subunits. The creation of strong contacts in opposing directions may act to further stabilize the ligand binding. This is in contrast to MII, which exhibits hydrogen bonding primarily along a single axis. Interestingly, the three bulky tryptophan residues of KTM do not make any strikingly obvious contributions that would lead to an explanation for the high sequence homology observed in the top results from GAMPMS, such as the conservation of Trp10 across all of the top 50 sequences. However, upon examination of the bound complex, it becomes apparent that the Trp10 side chain is stabilized deep in the largely hydrophobic inner portion of the binding pocket. The lesser, although significant, conservation of Trp1 and Trp15 is more difficult to explain but may result from the exclusion of a larger number of potentially destabilizing solvent molecules from the bound KTM by the bulky tryptophan side chains. Another interesting finding is that the Lys14 mutation of KTM does not play an important role in stabilizing the ligand despite the ability of charged lysine residues to readily form strong hydrogen-bonding interactions. The positioning of the ligand in the binding pocket and cumulative stabilizing interactions prevent K14 from forming strong contacts with any of the receptor residues. This discovery also agrees with the sequence homology of the top sequences displayed in Figure 3, where it can be seen that residue 14 has the lowest degree of homology of all the residues, suggesting that the functionality of this residue side chain is largely negated by the conformation of the ligand in the $\alpha_3\beta_2$-nAChR binding pocket.

The orientations of MII and KTM in the receptor binding pocket are noticeably different (Figure 8). As a result of the variations in ligand–receptor interactions, a slight rotation of KTM with respect to MII was observed. This positional change of KTM induced a potentially significant structural change in the nAChR. The dynamics and functionality of the biologically active pentameric transmembrane structure involves the closing of the C loops between adjacent subunits (labeled in Figure 8) upon binding of α-CTx.[51–53] The C loop of the α_3 subunit moved into much closer proximity to the β_2 subunit in the KTM simulation than was observed for MII, indicating tighter closure of the C loop upon KTM binding. The distance between receptor backbone atoms at the narrowest juncture was measured as approximately 13.2 Å for KTM binding compared with 18.1 Å for MII binding. This is nearly a 30% decrease in spacing between the α_3 C loop and the β_2 subunit. This reduction occurs despite the ~10% increase in molecular volume of the KTM mutant. The KTM binding paradigm may have a substantial impact on the biological function of the $\alpha_3\beta_2$-nAChR.

Calculations of binding free energies were performed for both MII and KTM using MD free energy perturbation methods. For comparison and also to validate the relative free energy calculations, the same calculations were carried out for two additional α-CTx's, PnIA and TxIA, which have been shown to have higher binding affinities for the $\alpha_3\beta_2$-nAChR than MII.[54,55] PnIA has nine residue variations from the MII sequence, while TxIA has eight different residues (Table 3). The PnIA and TxIA sequences are similar, with conservation at all but residues 5, 9, and 15. Only Ser4 is conserved across all four peptide sequences, and this is the only sequence similarity among KTM, PnIA, and TxIA, excluding the five nonmutable residues defined in the GAMPMS analysis.

As shown in Table 3, the calculated ΔG_{bind} for KTM was −45.59 kcal/mol, which is more than double that of MII (−20.42 kcal/mol). This difference corresponds to a significant increase in binding free energy of −25.17 kcal/mol. The relative binding free energies of the reference PnIA and TxIA peptides compared with MII were roughly half this magnitude, producing $\Delta\Delta G$ values of −11.11 and −11.77 kcal/mol, respectively. Although the calculated binding free energies of PnIA and TxIA are difficult to correlate with that of MII in absolute terms since there is no direct translation between ΔG_{bind} and experimentally obtained IC_{50} values, the relative ΔG_{bind} is in agreement with experimental results showing the significant predicted enhancement in binding affinity of these peptides for the $\alpha_3\beta_2$-nAChR.[54] The even greater affinity of KTM binding for the $\alpha_3\beta_2$-nAChR is clearly supported by the considerably larger calculated binding free energy.

To further validate the method of creating the consensus sequence from the top GAMPMS results, MD free energy simulations were performed on the top sequence shown in Table 2 in an equivalent manner. The sequence of WCCSRPGCYWTSHKWC differs from that of KTM at only three locations by the substitutions Y5R, S11T, and S13H. The calculated ΔG_{bind} was found to be −39.14 kcal/mol (ΔG_{bound} = −215.36 kcal/mol, ΔG_{solv} = −176.22 kcal/mol). Comparison of the values to those in Table 3 shows that while the binding affinity of this peptide ligand for the $\alpha_3\beta_2$-nAChR is superior to those of the native MII, PnIA, and TxIA, this ligand has a lower ΔG_{bind} than the consensus sequence KTM. This is evidence that high residue conservation among top peptides resulting from vast mutant library searches is a strong indicator of key amino acid residues contributing to enhanced binding affinity.

There are notable differences between the free energies from the GAMPMS and MD simulations (Tables 2 and 3). Such differences arise from the discrepancies in the methods used to obtain these values. In molecular docking experiments, there is limited flexibility in the ligand and receptor side chains, thus reducing the possibility that optimal binding interactions will be established and the ligand will find its most stable binding configuration. Although useful in ranking potential candidates, the estimated free energies obtained by molecular docking can only be used as approximations toward determining optimal ligands within the errors associated with these limitations. By subsequent analysis by molecular dynamics, the binding energies of ligands can be more carefully determined. MD simulations permit the sampling of ensemble interaction configurations while allowing for much greater flexibility in the molecular structures. Likewise, by the use of perturbative free energy simulations, more accurate values can be obtained by slowly turning off (or on) relevant binding interactions and using the appropriate statistical analyses. This results in a better representative model system from which the binding free energy can be calculated.

The GAMPMS search of 40.96 billion possible peptide sequences to find those with the greatest binding affinity for the $\alpha_3\beta_2$-nAChR produced a series of top results with high sequence homology using molecular docking to estimate the free energy of binding. The estimated ΔG_{bind} was nearly double that of the native α-CTx MII ligand. In comparison to a previous GAMPMS application to this system using a limited mutation space of 640 000, consistencies are evident in the resulting top peptide sequences from the two mutant libraries. Of those residues mutated in the peptide subset, amino acid conservation among

the top 10 mutants was seen in Tyr5 and Trp10, which are the same as in KTM and most of the top mutants from the comprehensive search. Similarities were seen with each of the other residues 9, 11, 12, and 15, showing partial conservation of the same mutations preferential in the generation of the KTM sequence. The predicted binding free energies obtained ranged from −20.66 to −21.07 kcal/mol, which is approximately 10% lower than for the peptide mutants shown in Table 2. The inclusion of additional mutable residues in the searchable mutant library provided further opportunity for optimization of the peptide binding affinity and effectively demonstrated consistency in favored mutations at corresponding residue positions.

The high sequence homology among the top peptide ligand sequences produced by GAMPMS are evidence of important mutations contributing to optimal predicted binding affinity. Since the differences among the estimated binding free energies for the top results from molecular docking were within the error range of these methods, a definitive peptide sequence with the greatest affinity for $\alpha_3\beta_2$-nAChR could not be immediately identified, although each was substantially more likely to exhibit stronger binding than MII. A consensus sequence, KTM, was taken from the top 50 peptide sequences on the basis of sequence homology, selecting the most frequently reached amino acid among each of the mutable residues. Basing the KTM sequence on residue conservation, as opposed to the absolute AutoDock scores accompanied by large relative errors, puts emphasis on which amino acid residues most favorably contribute to an optimal binding interaction. Through further investigation by molecular dynamics simulations, it was demonstrated that the binding affinity of KTM for the $\alpha_3\beta_2$-nAChR was much greater than those of MII, the known α-CTx's PnIA and TxIA, and the top resulting sequences from GAMPMS.

Identifying ligands with greater biological activities toward targeted receptors could aid in the development of therapeutics with either inhibiting or stimulating effects. In the case of the nAChR, such discoveries could lead to innovative new treatments for neurodegenerative diseases. These discoveries may also provide valuable insight into the essential biological function of the targeted receptor. The structure–function relationship of a peptide receptor can be exceedingly complicated, and those receptor structures whose activity involves several dynamical contributions, such as the trans-membrane structures of the nAChR, only increase this complexity. Any information about the intricate interactions of ligand–receptor complexes is a step further in developing important targeted therapeutics.

Conclusions

The efficiency of genetic algorithms to substantially reduce the sample population size through evolutionary selection criteria has been demonstrated in this study. The implementation of GAMPMS has produced an α-CTx MII analogue with optimal binding to the $\alpha_3\beta_2$-nAChR by heuristically searching the set of all possible amino acid residue combinations. The resulting consensus mutant peptide, KTM, was shown to have considerably higher binding affinity for the $\alpha_3\beta_2$-nAChR than the highly studied reference α-CTx MII. Molecular dynamics free energy calculations produced a ΔG_{bind} for KTM that was more than double that of MII, in agreement with the estimates of binding free energy provided by initial molecular docking results.

This study demonstrates the utility of GAMPMS to search exceptionally large and otherwise intractable mutant libraries for sequences that possesses greater binding affinities for target receptors. The GAMPMS search of 40.96 billion possible peptide sequences to find those with the greatest binding affinity for the $\alpha_3\beta_2$-nAChR produced a series of top results with high sequence homology and estimated ΔG_{bind} values twice that of the potent MII ligand. The binding affinity of the resulting consensus sequence was confirmed by more intensive molecular dynamics simulations. While the identification of ligands with greater affinities for targeted receptors is undoubtedly advantageous for the development of therapeutics, the implementation of advanced searching algorithms, such as GAMPMS, will aid in expediting the process of new treatment discovery.

Acknowledgments

This research made use of the resources of the High Performance Computing Center at Idaho National Laboratory, which is supported by the Office of Nuclear Energy of the U.S. Department of Energy under Contract DE-AC07-05ID14517. This material is based in part upon work supported by the NSF #1229709. This project was supported by NIH #P20GM109095, NSF #0619793 and #0923535, and the M.J. Murdock Charitable Trust.

References

1. Picciotto MR, Zoli M. Neuroprotection via nAChRs: The Roleof nAChRs in Neurodegenerative Disorders Such as Alzheimer's andParkinson's Disease. Front Biosci. 2008; 13:492–504. [PubMed: 17981563]
2. Morens DM, Davis JW, Grandinetti A, Ross GW, Popper JS, White LR. Epidemiologic Observations on Parkinson's Disease: Incidence and Mortality in a Prospective Study of Middle-Aged Men. Neurology. 1996; 46:1044–1050. [PubMed: 8780088]
3. Quik M, Wonnacott S. $\alpha_6\beta_2$ and $\alpha_4\beta_2$ Nicotinic Acetylcholine Receptors as Drug Targets for Parkinson's Disease. Pharmacol Rev. 2011; 63:938–966. [PubMed: 21969327]
4. Buckingham SD, Jones AK, Brown LA, Sattelle DB. Nicotinic Acetylcholine Receptor Signaling: Roles in Alzheimer's Disease and Amyloid Neuroprotection. Pharmacol Rev. 2009; 61:39–61. [PubMed: 19293145]
5. Perry EK, Martin-Ruiz CM, Court JA. Nicotinic Receptor Subtypes in Human Brain Related to Aging and Dementia. Alcohol. 2001; 24:63–68. [PubMed: 11522424]
6. Levin ED, McClernon FJ, Rezvani AH. Nicotinic Effects on Cognitive Function: Behavioral Characterization, Pharmacological Specification, and Anatomic Localization. Psychopharmacol. 2006; 184:523–539.
7. Fratiglioni L, Wang HX. Smoking and Parkinson's and Alzheimer's Disease: Review of the Epidemiological Studies. Behav Brain Res. 2000; 113:117–120. [PubMed: 10942038]
8. Rezvani K, Teng Y, Shim D, De Biasi M. Nicotine Regulates Multiple Synaptic Proteins by Inhibiting Proteasomal Activity. J Neurosci. 2007; 27:10508–10519. [PubMed: 17898222]
9. Kane JK, Konu O, Ma JZ, Li MD. Nicotine Coregulates Multiple Pathways Involved in Protein Modification/Degradation in Rat Brain. Mol Brain Res. 2004; 132:181–191. [PubMed: 15582157]
10. Salminen O, Drapeau JA, McIntosh JM, Collins AC, Marks MJ, Grady SR. Pharmacology of α-Conotoxin MII-Sensitive Subtypes of Nicotinic Acetylcholine Receptors Isolated by Breeding of Null Mutant Mice. Mol Pharmacol. 2007; 71:1563–1571. [PubMed: 17341654]
11. Jacob RB, McDougal OM. The M-Superfamily of Conotoxins: A Review. Cell Mol Life Sci. 2010; 67:17–27. [PubMed: 19705062]
12. Sambasivarao VS, Roberts J, Bharadwaj VS, Slingsby JG, Rohleder C, Mallory C, Groome JR, McDougal OM, Maupin CM. Acetycholine Promotes Binding of alpha-Conotoxin MII for $\alpha_3\beta_2$ Nicotinic Acetylcholine Receptors. ChemBioChem. 2014; 15:413–424. [PubMed: 24420650]

13. McIntosh JM, Azam L, Staheli S, Dowell C, Lindstrom JM, Kuryatov A, Garrett JE, Marks MJ, Whiteaker P. Analogs of α-Conotoxin MII are Selective for α_6-Containing Nicotinic Acetylcholine Receptors. Mol Pharmacol. 2004; 65:944–952. [PubMed: 15044624]
14. Cartier GE, Yoshikami D, Gray WR, Luo S, Olivera BM, McIntosh JM. A New α-Conotoxin which Targets $\alpha_3\beta_2$ Nicotinic Acetylcholine Receptors. J Biol Chem. 1996; 271:7522–7528. [PubMed: 8631783]
15. Kulak JM, Nguyen TA, Olivera BM, McIntosh JM. α-Conotoxin MII Blocks Nicotine-Stimulated Dopamine Release in Rat Striatal Synaptosomes. J Neurosci. 1997; 17:5263–5270. [PubMed: 9204910]
16. Dutertre S, Lewis RJ. Computational Approaches to Understand α-Conotoxin Interactions at Neuronal Nicotinic Receptors. Eur J Biochem. 2004; 271:2327–2334. [PubMed: 15182348]
17. Kompella SN, Cuny H, Hung A, Adams DJ. Molecular Basis for Differential Sensitivity of α-Conotoxin RegIIA at Rat and Human Neuronal Nicotinic Acetylcholine Receptors. Mol Pharmacol. 2015; 88:993–1001. [PubMed: 26438212]
18. Papineni RV, Sanchez JU, Baksi K, Willcockson IU, Pedersen SE. Site-Specific Charge Interactions of Alpha-Conotoxin MI with the Nicotinic Acetylcholine Receptor. J Biol Chem. 2001; 276:23589–23598. [PubMed: 11323431]
19. Harvey SC, McIntosh JM, Cartier GE, Maddox FN, Luetje CW. Determinants of Specificity for α-Conotoxin MII on $\alpha_3\beta_2$ Neuronal Nicotinic Receptors. Mol Pharmacol. 1997; 51:336–342. [PubMed: 9203640]
20. Grishin AA, Cuny H, Hung A, Clark RJ, Brust A, Akondi K, Alewood PF, Craik DJ, Adams DJ. Identifying Key Amino Acid Residues that Affect α-Conotoxin AuIB Inhibition of $\alpha_3\beta_4$ Nicotinic Acetylcholine Receptors. J Biol Chem. 2013; 288:34428–34442. [PubMed: 24100032]
21. Bordia T, Grady SR, McIntosh JM, Quik M. Nigrostriatal damage preferentially decreases a subpopulation of $\alpha_6\beta_2$ nAChRs in mouse, monkey, and Parkinson's disease striatum. Mol Pharmacol. 2007; 72:52–61. [PubMed: 17409284]
22. Long T, McDougal OM, Andersen T. GAMPMS: Genetic Algorithm Managed Peptide Mutant Screening. J Comput Chem. 2015; 36:1304–1310. [PubMed: 25975567]
23. Sheridan RP, Kearsley SK. Using a Genetic Algorithm to Suggest Combinatorial Libraries. J Chem Inf Model. 1995; 35:310–320.
24. Sheridan RP, San Feliciano SG, Kearsley SK. Designing Targeted Libraries with Genetic Algorithms. J Mol Graphics Modell. 2000; 18:320–334.
25. Fonseca CM, Fleming PJ. An Overview of Evolutionary Algorithms in Multiobjective Optimization. Evol Comput. 1995; 3:1–16.
26. Gillet VJ, Khatib W, Willett P, Fleming PJ, Green DVS. Combinatorial Library Design Using a Multiobjective Genetic Algorithm. J Chem Inf Comput Sci. 2002; 42:375–385. [PubMed: 11911707]
27. Morris GM, Goodsell DS, Halliday RS, Huey R, Hart WE, Belew RK, Olson AJ. Automated Docking Using a Lamarckian Genetic Algorithm and Empirical Binding Free Energy Function. J Comput Chem. 1998; 19:1639–1662.
28. Huey R, Morris GM, Olson AJ, Goodsell DS. A Semi-Empirical Free Energy Force Field with Charge-Based Desolvation. J Comput Chem. 2007; 28:1145–1152. [PubMed: 17274016]
29. Bullock C, Cornia N, Jacob R, Remm A, Peavey T, Weekes K, Mallory C, Oxford JT, McDougal OM, Andersen TL. DockoMatic 2.0: High Throughput Inverse Virtual Screening and Homology Modeling. J Chem Inf Model. 2013; 53:2161–2170. [PubMed: 23808933]
30. The UniProt Consortium. UniProt: a Hub for Protein Information. Nucleic Acids Res. 2015; 43:D204–D212. [PubMed: 25348405]
31. Unwin N. Refined Structure of the Nicotinic Acetylcholine Receptor at 4Å Resolution. J Mol Biol. 2005; 346:967–989. [PubMed: 15701510]
32. Sali A, Blundell TL. Comparative Protein Modelling by Satisfaction of Spatial Restraints. J Mol Biol. 1993; 234:779–815. [PubMed: 8254673]
33. Xu J, Berger B. Fast and Accurate Algorithms for Protein Side-Chain Packing. J Assoc Comput Mach. 2006; 53:533–557.

34. Hess B, Kutzner C, van der Spoel D, Lindahl E. GROMACS 4: Algorithms for Highly Efficient, Load-Balanced, and Scalable Molecular Simulation. J Chem Theory Comput. 2008; 4:435–447. [PubMed: 26620784]
35. van der Spoel D, Lindahl E, Hess B, Groenhof G, Mark AE, Berendsen HJC. GROMACS: Fast, Flexible, and Free. J Comput Chem. 2005; 26:1701–1719. [PubMed: 16211538]
36. Berendsen HJC, van der Spoel D, van Drunen R. GROMACS: A Message-Passing Parallel Molecular Dynamics Implementation. Comput Phys Commun. 1995; 91:43–56.
37. Sorin EJ, Pande VS. Exploring the Helix-Coil Transition via All-Atom Equilibrium Ensemble Simulations. Biophys J. 2005; 88:2472–2493. [PubMed: 15665128]
38. DePaul AJ, Thompson EJ, Patel SS, Haldeman K, Sorin EJ. Equilibrium Conformational Dynamics in an RNA Tetraloop from Massively Parallel Molecular Dynamics. Nucleic Acids Res. 2010; 38:4856–4867. [PubMed: 20223768]
39. Duan Y, Wu C, Chowdhury S, Lee MC, Xiong G, Zhang W, Yang R, Cieplak P, Luo R, Lee T, Caldwell J, Wang J, Kollman P. A Point-Charge Force Field for Molecular Mechanics Simulations of Proteins Based on Condensed-Phase Quantum Mechanical Calculations. J Comput Chem. 2003; 24:1999–2012. [PubMed: 14531054]
40. Jorgensen WL, Chandrasekhar J, Madura JD, Impey RW, Klein ML. Comparison of Simple Potential Functions for Simulating Liquid Water. J Chem Phys. 1983; 79:926–935.
41. Bussi G, Donadio D, Parrinello M. Canonical Sampling Through Velocity Rescaling. J Chem Phys. 2007; 126:014101. [PubMed: 17212484]
42. Parrinello M, Rahman A. Polymorphic Transitions in Single Crystals: A New Molecular Dynamics Method. J Appl Phys. 1981; 52:7182–7190.
43. Nose S, Klein ML. Constant Pressure Molecular Dynamics for Molecular Systems. Mol Phys. 1983; 50:1055–1076.
44. Hess B, Bekker H, Berendsen HJC, Fraaije JGEM. LINCS: A Linear Constraint Solver for Molecular Simulations. J Comput Chem. 1997; 18:1463–1472.
45. Darden T, York D, Pedersen L. Particle Mesh Ewald: An Nlog(N) Method for Ewald Sums in Large Systems. J Chem Phys. 1993; 98:10089–10092.
46. Essmann U, Perera L, Berkowitz ML, Darden T, Lee H, Pedersen LG. A Smooth Particle Mesh Ewald Potential. J Chem Phys. 1995; 103:8577–8592.
47. Beutler TC, Mark AE, van Schaik RC, Gerber PR, van Gunsteren WF. Avoiding Singularities and Numerical Instabilities in Free Energy Calculations Based on Molecular Simulations. Chem Phys Lett. 1994; 222:529–539.
48. Pham TT, Shirts MR. Identifying Low Variance Pathways for Free Energy Calculations of Molecular Transformations in Solution Phase. J Chem Phys. 2011; 135:034114. [PubMed: 21786994]
49. Bennett CH. Efficient Estimation of Free Energy Differences from Monte Carlo Data. J Comput Phys. 1976; 22:245–268.
50. Pan Y, Huang N, Cho S, MacKerell AD Jr. Consideration of Molecular Weight during Compound Selection in Virtual Target-Based Database Screening. J Chem Inf Comput Sci. 2003; 43:267–272. [PubMed: 12546562]
51. Celie PHN, Klaassen RV, van Rossum-Fikkert SE, van Elk R, van Nierop P, Smit AB, Sixma TK. Crystal Structure of Acetylcholine-Binding Protein form Bulinus trucatus Reveals the Conserved Structural Scaffold and Sites of Variation in Nicotinic Acetylcholine Receptors. J Biol Chem. 2005; 280:26457–26466. [PubMed: 15899893]
52. Hansen SB, Sulzenbacher G, Huxford T, Marchot P, Taylor P, Bourne Y. Structures of Aplysia AChBP Complexes With Nicotinic Agonists and Antagonists Reveal Distinct Binding Interfaces and Conformations. EMBO J. 2005; 24:3635–3646. [PubMed: 16193063]
53. Cheng X, Wang H, Grant B, Sine SM, McCammon JA. Targeted Molecular Dynamics Study of C-Loop Closure and Channel Gating in Nicotinic Receptors. PLoS Comput Biol. 2006; 2:e134. [PubMed: 17009865]
54. Dutertre S, Ulens C, Buttner R, Fish A, van Elk R, Kendel Y, Hopping G, Alewood PF, Schroeder C, Nicke A, Smit AB, Sixma TK, Lewis RJ. AChBP-Targeted α-Conotoxin Correlates Distinct

Binding Orientations with nAChR Subtype Selectivity. EMBO J. 2007; 26:3858–3867. [PubMed: 17660751]

55. Hopping G, Wang CI, Hogg RC, Nevin ST, Lewis RJ, Adams DJ, Alewood PF. Hydrophobic Residues at Position 10 of α-Conotoxin PnIA Influence Subtype Selectivity Between α_7 and $\alpha_3\beta_2$ Neuronal Acetylcholine Receptors. Biochem Pharmacol. 2014; 91:534–542. [PubMed: 25101833]

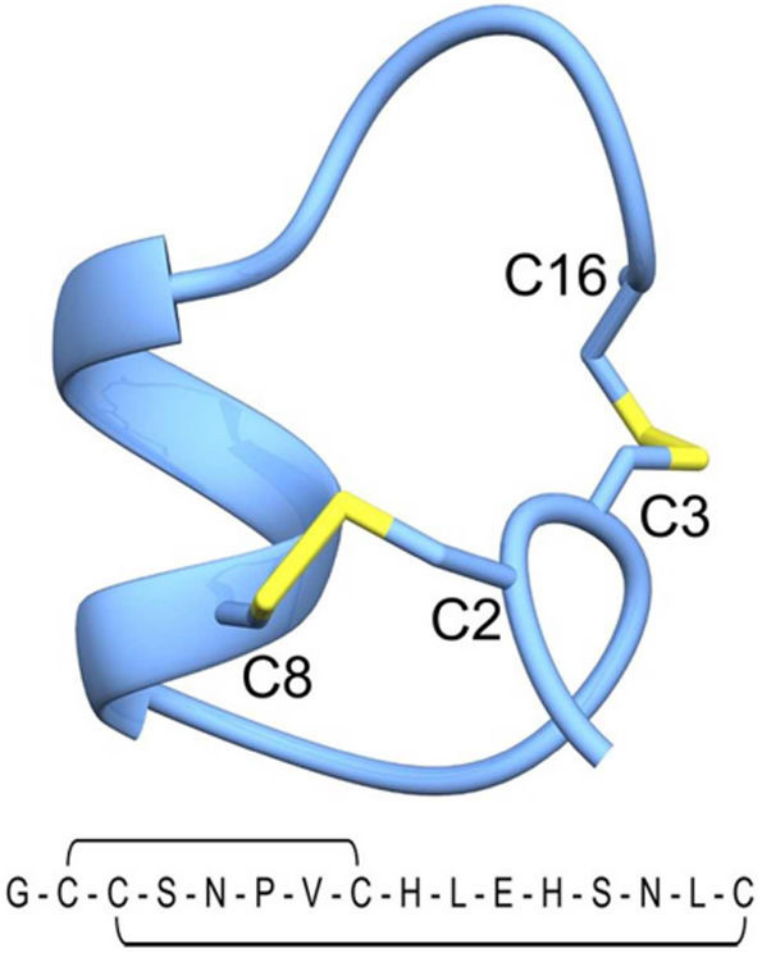

Figure 1.
Peptide structure and sequence of α-CTx MII.

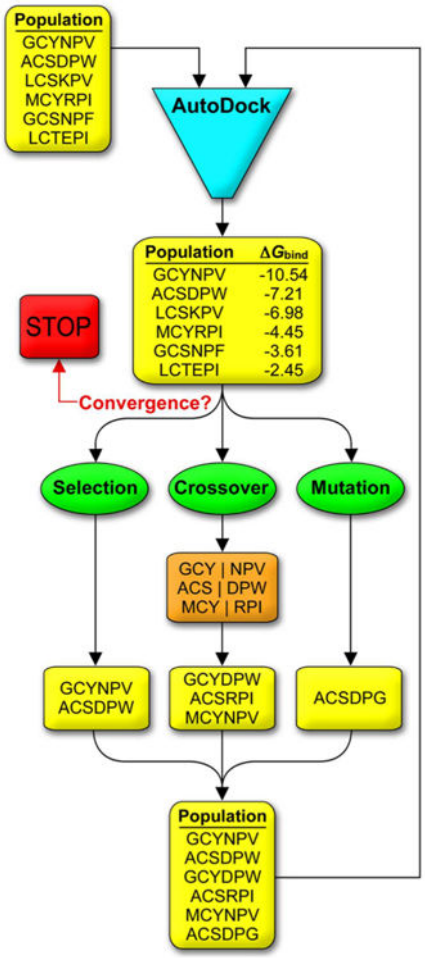

Figure 2.
Schematic representation of the GAMPMS workflow.

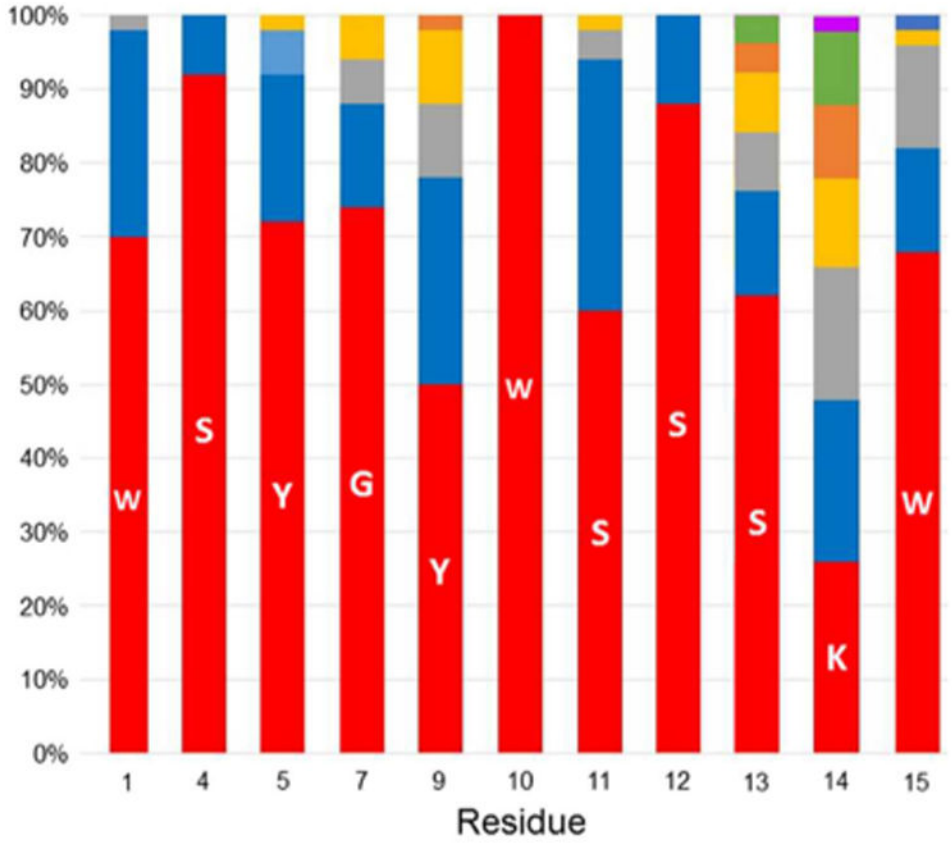

Figure 3.
Relative frequencies of amino acid residues present in the top 50 sequences obtained from GAMPMS.

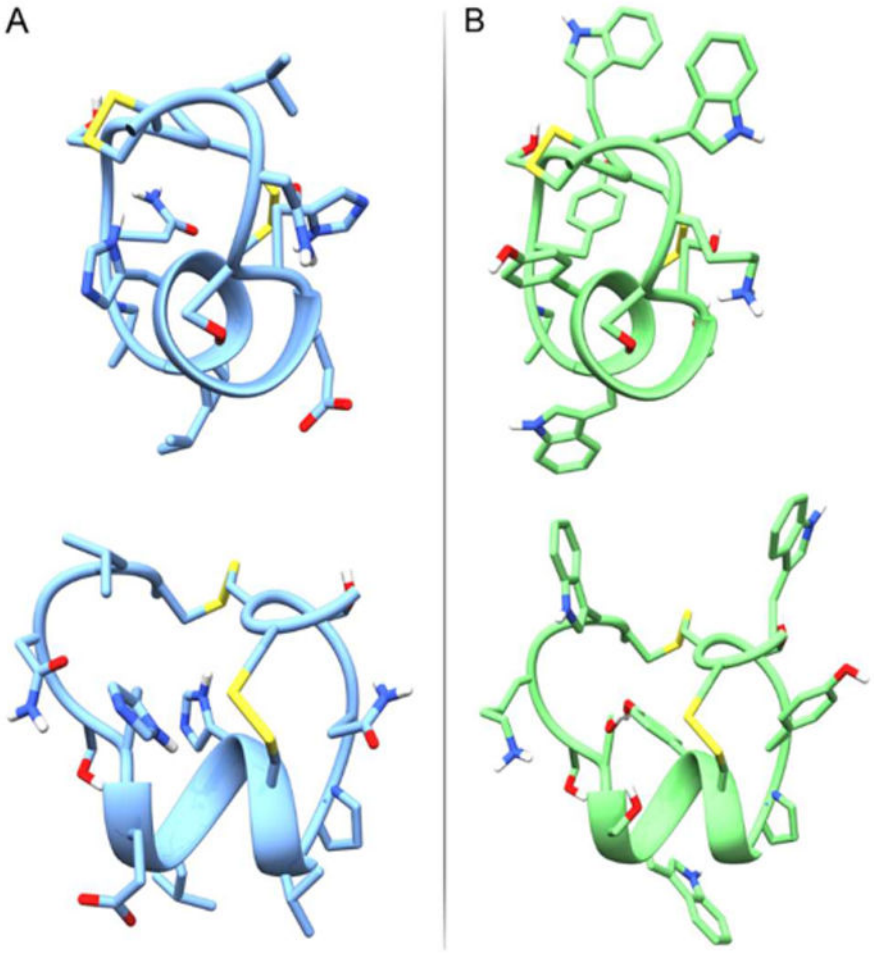

Figure 4.
Peptide structures of (A) α-CTx MII and (B) the consensus sequence from the GAMPMS search results (KTM).

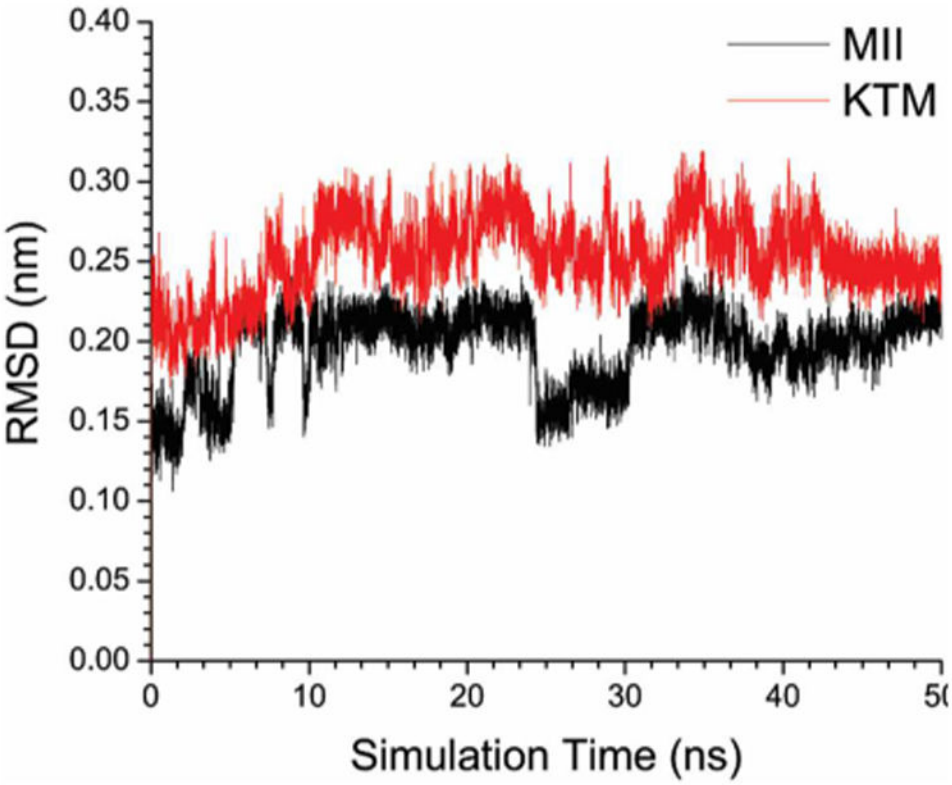

Figure 5.

Root-mean-square deviations (RMSDs) of ligand atomic positions over the initial 50 ns MD simulations for α-CTx MII (black) and KTM (red).

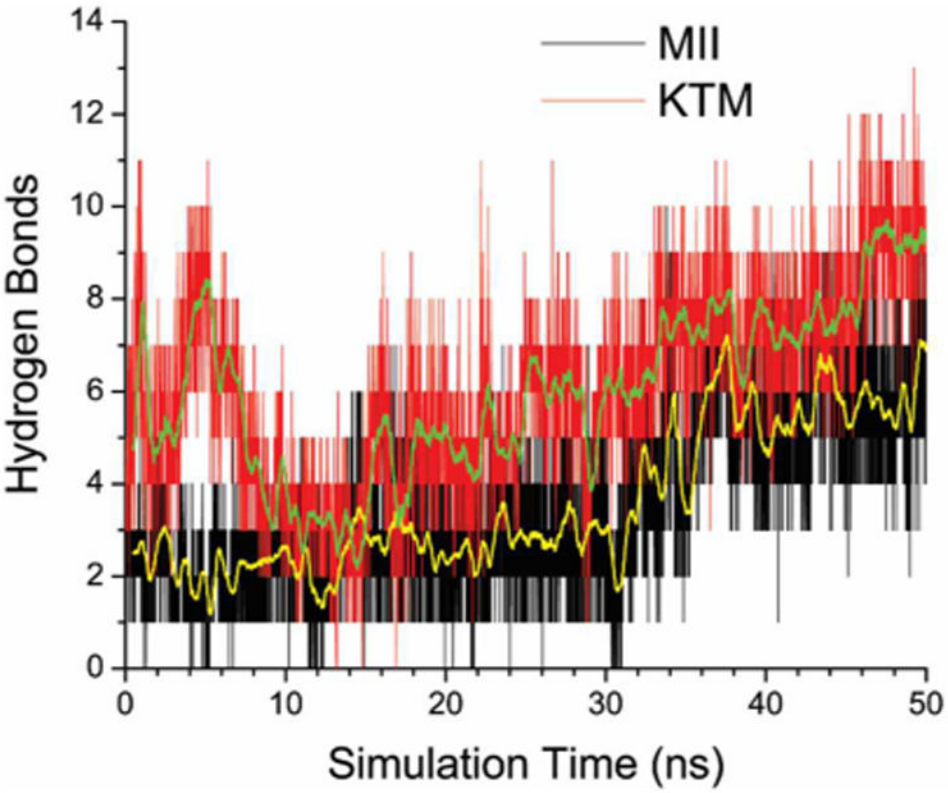

Figure 6.

Numbers of hydrogen bonds formed between the ligands and the nAChR over the 50 ns MD simulations. Running averages of 500 ps are shown in yellow and green for the MII and KTM ligands, respectively.

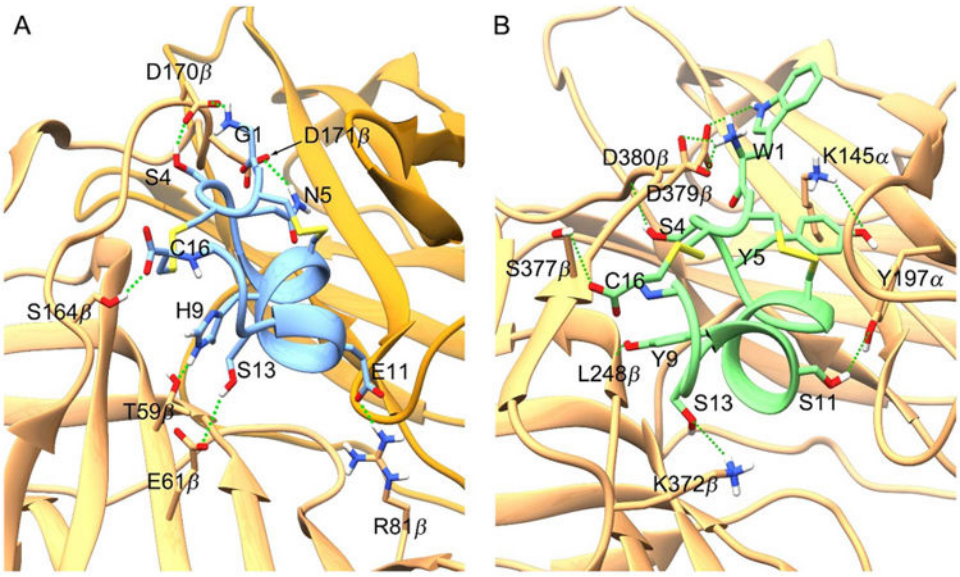

Figure 7.

Hydrogen-bonding interactions of the $\alpha_3\beta_2$-nAChR with (A) MII and (B) KTM revealed from MD simulations of GAMPMS docked structures.

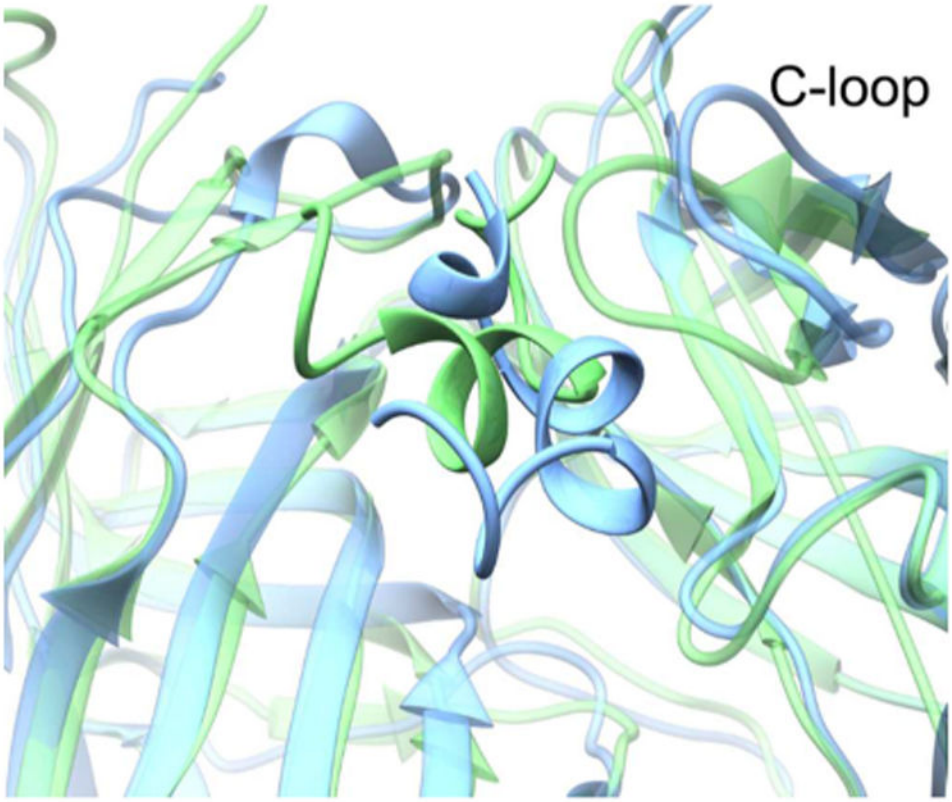

Figure 8.
Overlay of MII (blue) and KTM (green) in the $\alpha_3\beta_2$-nAChR binding pocket.

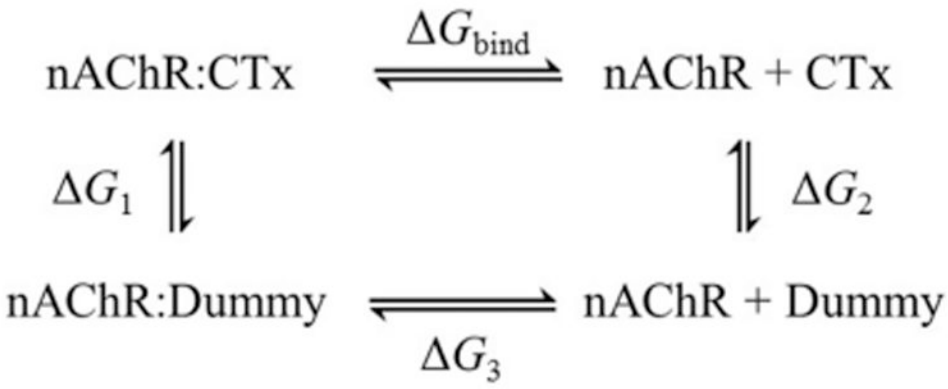

Scheme 1.
Thermodynamic Cycle Used in MD Binding Free Energy Calculations

Table 1

α-CTx MII Mutant Ligand Library, Defined as a Base Peptide and a Set of Mutation Constraints

mutable residue	substitutable amino acids
G1	G A V L I M W F
S4	S T Y N Q D E K R H
N5	S T Y N Q D E K R H
V7	G A V L I M W F
H9	S T Y N Q D E K R H
L10	G A V L I M W F
E11	S T Y N Q D E K R H
H12	S T Y N Q D E K R H
S13	S T Y N Q D E K R H
N14	S T Y N Q D E K R H
L15	G A V L I M W F

Table 2

Top 10 Peptide Sequences with the Highest Binding Affinities for the nAChR $\alpha_3\beta_2$-Isoform As Identified by GAMPMS

peptide sequence[a]	Δ*G*bind[b]	ΔΔ*G*[c]
W**CC**S**P**G**C**YWT**S**HKW**C**	−23.45	−11.07
G**CC**S**YP**F**C**SWTN**S**KW**C**	−23.38	−11.00
F**CC**S**YP**G**C**YWTNNKW**C**	−23.12	−10.74
W**CC**S**YP**G**C**SWSN**S**RW**C**	−22.71	−10.33
W**CC**S**HP**G**C**YWSSH**N**W**C**	−22.70	−10.32
F**CC**S**YP**V**C**YWSN**S**KW**C**	−22.65	−10.27
F**CC**TY**P**G**C**YWTSRTA**C**	−22.64	−10.26
F**CC**S**HP**G**C**YWSSHKW**C**	−22.52	−10.14
W**CC**S**YP**A**C**YWQS**S**TA**C**	−22.39	−10.01
W**CC**S**RP**G**CH**WSS**S**TW**C**	−22.26	−9.88
G**CC**S**NP**V**CH**LEHSNL**C** (MII)	−12.38	–

[a]Residues conserved from the native sequence are set in bold type.

[b]Estimated from the AutoDock scoring function, in kcal/mol.

[c]Free energy of binding relative to MII, in kcal/mol.

Table 3

Free Energies of Binding for KTM, MII, PnIA, and TxIA with the $\alpha_3\beta_2$-nAChR Obtained from Molecular Dynamics Free Energy Perturbation Simulations[a]

peptide	sequence	Δ*G*bound	Δ*G*solv	Δ*G*bind	ΔΔ*G*
KTM	WCCSYPGCYWSSSKWC	−216.78 (1.02)	−171.20 (1.13)	−45.59 (1.07)	−25.17
TxIA	GCCSRPPCIANNPDLC	−201.33 (1.02)	−169.13 (1.09)	−32.20 (1.05)	−11.77
PnIA	GCCSLPPCAANNPDYC	−199.57 (1.28)	−168.04 (1.10)	−31.53 (1.51)	−11.11
MII	GCCSNPVCHLEHSNLC	−191.30 (1.12)	−170.89 (0.80)	−20.42 (0.97)	–

[a]Δ*G* values are given in kcal/mol; errors are shown in parentheses.